

Even denominator fractional quantum Hall states in the zeroth Landau level of monolayer-like band of ABA trilayer graphene

Tanima Chanda^{1†}, Simrandeep Kaur^{1†}, Harsimran Singh¹, Kenji Watanabe², Takashi Taniguchi³, Manish Jain¹, Udit Khanna⁴, Ajit C. Balam^{5,6}, and Aveek Bid^{1,*}

¹*Department of Physics, Indian Institute of Science, Bangalore 560012, India*

²*Research Center for Electronic and Optical Materials,*

National Institute for Materials Science,

1-1 Namiki, Tsukuba 305-0044, Japan

³*Research Center for Materials Nanoarchitectonics,*

National Institute for Materials Science,

1-1 Namiki, Tsukuba 305-0044, Japan

⁴*Theoretical Physics Division, Physical Research Laboratory,*

Navrangpura, Ahmedabad-380009, India

⁵*Institute of Mathematical Sciences, CIT Campus, Chennai 600113, India*

⁶*Homi Bhabha National Institute, Training School Complex,*

Anushaktinagar, Mumbai 400094, India

[†]*These authors contributed equally*

Abstract

The fractional quantum Hall (FQH) effect is a macroscopic manifestation of strong electron-electron interactions. Even denominator FQH states (FQHSs) at half-filling are particularly interesting as they are predicted to host non-Abelian excitations with non-trivial braiding statistics. Such states are predominantly observed in the $N = 1$ Landau level (LL) of semiconductors such as GaAs. In this Letter, we report the unanticipated observation of even-denominator FQHSs in the $N = 0$ LL of ABA trilayer graphene (TLG), a system characterized by tunable LL mixing and the absence of inversion symmetry. Notably, we find robust FQHSs at $\nu = 5/2$ and $\nu = 7/2$ when two LLs, originating from a monolayer-like band of TLG with different isospin indices, cross each other. These are flanked by the Levin-Halperin daughter states at $\nu = 7/13$ and $\nu = 9/17$, respectively, and further away, the standard series of Jain-sequence of composite fermions (CFs) is observed. The even-denominator FQHSs and their accompanying daughter states become stronger with increasing magnetic fields while concomitantly a weakening of the CF states is observed. We posit that the absence of inversion symmetry in the system gives rise to additional isospin interactions which enhance LL mixing and soften the short-range part of the Coulomb repulsion stabilizing the even-denominator FQHSs. In addition, we demonstrate that these states, along with their daughter states, can be finely tuned with an external displacement field that serves as an important tool to control the LL mixing in the system.

I. INTRODUCTION

The fractional quantum Hall effect (FQHE) [1–3] provides a striking visualization of strong electron-electron interactions in condensed matter systems. Among these, even denominator FQHSs are particularly exciting due to their potential to host quasiparticles that obey non-Abelian statistics [4–13]. A well-known example is the $\nu = 5/2$ state [14–16] of two-dimensional electron systems in GaAs [17–20] quantum wells [21, 22]. These states are typically observed in a two-dimensional electron system at half-filling of the second ($N = 1$) LL [21, 23–34], where a node in the wavefunction softens Coulomb repulsion, allowing pairing of electron-vortex composites called composite fermions (CFs) [35, 36]. Conversely, in the lowest ($N = 0$) LL, strong Coulomb repulsion stabilizes weakly interacting CFs, which form a gapless CF Fermi liquid (CFFL) [37] at half-filling instead of an FQHS. However, at least two mechanisms to bypass this general principle exist, where the suppression of Coulomb repulsion at short distances facilitates the emergence of

* aveek@iisc.ac.in

even denominator FQHSs in the $N = 0$ LL. First, in quantum wells with a large width or high carrier density, the intra-LL interaction is weakened due to the spread of the single-particle wavefunction in the out-of-plane direction, leading to the appearance of the $\nu = 1/2$ and $\nu = 1/4$ FQHS [20, 38–43]. Second, in systems with large LL mixing, the electrons can access other LLs [44]. This additional degree of freedom suppresses the repulsion at short distances and results in a FQHS [45, 46]. The recent observation of $\nu = 3/4$ FQHS in the $N = 0$ LL of bilayer graphene [47] likely has to do with LL mixing as well, though the exact mechanism underlying its origin remains unclear.

In this Letter, we report the observation of single-component [43] even-denominator FQHSs at $\nu = 5/2$ and $\nu = 7/2$ in Bernal stacked trilayer graphene (TLG) [48–51]. Along with the even-denominator states, we identify Levin-Halperin daughter states [52] in the vicinity of half-filling, which suggests that the even-denominator FQHS that we observe at $7/2$ ($5/2$) is in the Moore-Read Pfaffian (anti-Pfaffian) [6, 53, 54] universality class. The even-denominator FQHS and their associated daughter states grow stronger as the magnetic field increases while the CF states weaken simultaneously. These phases arise in the $N = 0$ orbital of the monolayer-like (MLL) band in the regime where two symmetry-broken LLs with different isospin indices are close in energy. LL mixing among these two levels is significantly enhanced when the single-particle gap between them is small, suppressing the short-range repulsion and stabilizing the paired CF state over the CFFL. Our findings are in contrast to the lack of incompressible states observed at half-filling in the $N = 0$ levels of BLG, despite the convergence of LLs with different isospins in energy within that system [28]. We conjecture that this distinction arises from the lack of inversion symmetry in TLG, which introduces additional lattice-scale couplings that promote LL mixing and stabilize the even-denominator FQHS.

II. RESULTS

Dual graphite-gated hexagonal boron nitride (hBN)-encapsulated TLG devices were fabricated using a standard dry transfer method [55–57]. The two gates enable simultaneous control of the number density n and the displacement field perpendicular to the plane of the device D (Supplementary Note 1) [58]. All measurements are carried out at $T = 20$ mK unless stated otherwise. Fig. 1(a–b) show the measured longitudinal resistance R_{xx} and transverse Hall conductance G_{xy} over the filling factor range $\nu = 2 - 3$ and $\nu = 3 - 4$, respectively, at a perpendicular magnetic

field $B = 12$ T, and a finite electric displacement field D . The most exciting feature of these plots is the appearance of even-denominator FQHSs at $\nu = 5/2$ and $\nu = 7/2$, evidenced by the strong dip in R_{xx} and well-developed half-integer plateaus in G_{xy} . The FQHS at $\nu = 7/2$ is accompanied by its Levin-Halperin daughter state at $\nu = 7/13$. Furthermore, there is a very weak indication of $\nu = 8/17$, but it is not strong enough to conclusively determine if $\nu = 7/2$ is in the Moore-Read Pfaffian or Halperin-331 phase [52, 59]. We also notice the $\nu = 9/17$ daughter state on one flank of the $\nu = 5/2$. Since one of the candidate parents of $\nu = 9/17$ – the Halperin-113 state – is not an FQHS [60, 61], the $5/2$ state likely resides in the anti-Pfaffian phase [52, 59], which is its other candidate parent. In this Letter, we focus on the physics of the $\nu = 7/2$ state; data for $\nu = 5/2$ are presented in Supplementary Information.

The magnetic field evolution of the longitudinal resistance R_{xx} and Hall conductance G_{xy} acquired at $D = -0.079$ V/nm are presented in Fig. 1(c) and (d). With increasing magnetic field B , the plateau at $G_{xy} = 7/2(e^2/h)$ become better defined. Concomitantly, the $\nu = 7/13$ state becomes more prominent than the Jain states. The enhancement of the $\nu = 7/13$ with increasing stability of the $7/2$ state is significant as this state corresponds to the simplest hierarchical daughter states of the $\nu = 7/2$ Pfaffian state or (331) state [52]. This observation points to a possible topological phase transition between the Jain sequence of CF FQHS and the daughter states of $\nu = 7/2$. Similar findings were recently reported in wide-quantum wells in GaAs [42].

Fig 2(a) is the contour plot of R_{xx} as a function of filling factor ν and displacement field D . The even denominator state at $\nu = 7/2$ appears only over a small, finite range of D (marked by the white dashed rectangle). Fig 2(b) shows the stability diagram of $\nu = 7/2$ (parameterized by $\Delta R_{xx}/R_0$) in the B - D plane (Supplementary Note 4). With the increasing $|D|$, the range of B -values hosting the $7/2$ state shifts to lower values.

Fig. 2(c) plots the Landau spectrum at $B = 12$ T, calculated using the tight-binding model based on the Slonczewski-Weiss-McClure model [62, 63] as a function of energy E and interlayer potential difference Δ_1 (Supplementary Note 6). We use the notation $LL_M^{\beta\gamma}$ with β , the orbital index and γ , the valley index of the LL, while \uparrow, \downarrow to denote the spins. A finite D (or equivalently Δ_1) breaks the mirror symmetry of the outer layers of the TLG, leading to multiple LL crossings. As Δ_1 increases, the LLs $LL_M^{0+ \uparrow}$ and $LL_M^{0- \downarrow}$ from different valleys of ML-like band approach each other and intersect around $\Delta_1 = 6.7$ meV ($D \sim 0.08$ V/nm). The red-shaded region indicates this regime in the figure. Interestingly, it is exactly at these values of B and D , $\nu = 7/2$ forms. The calculated crossing point of $LL_M^{0+ \uparrow}$ and $LL_M^{0- \downarrow}$ are marked by white-filled circles in Fig 2(c).

The locus of these points exactly tracks the experimentally estimated $B - D$ values where $7/2$ is observed to be the most robust. Similarly $LL_M^{0+} \uparrow$ and $LL_M^{0-} \uparrow$ bands seem to cross at approximately $\Delta_1 = 8.3$ meV ($D \sim 0.097$ V/nm), indicated by the blue shaded region. This is the value of D at which the $\nu = 5/2$ state forms (see Supplementary Note 3).

Fig. 2(e) compares the thermal activation gap of $\nu = 4$, Δ_{LL4} and $\nu = 7/2$, $\Delta_{7/2}$ with D at $B = 13$ T. We observe that within the D range where $\Delta_{7/2}$ peaks, Δ_{LL4} (excitation gap between $LL_M^{0-} \downarrow$ and $LL_M^{0+} \uparrow$) experiences a sharp decline, decreasing to nearly a quarter of its value at $D = 0$. This correlation suggests a strong causal relation between the LL crossing of $LL_M^{0-} \uparrow$ and $LL_M^{0+} \downarrow$ and the formation of $7/2$ state.

We now look closer at the Jain sequence of FQHS around $\nu = 7/2$. Fig. 3(a–c) show plots of R_{xx} measured over the T -range 20 mK to 1.1 K, at magnetic fields $B = 6.5$ T, $B = 9$ T, and $B = 12$ T, respectively. At the lowest B fields, $\nu = 7/2$ FQHS is absent, and we have particle-hole symmetry (PHS) around half-filling. This can be seen from the Arrhenius plots in Fig.3(d) whose slopes yield the activation energy gap Δ_ν – the gaps are identical for $\nu = 10/3$ and its hole-conjugate state $\nu = 11/3$. With increasing B , the resistance dip at $\nu = 7/2$ strengthens [see Fig. 3(b)]. Concurrently, the Arrhenius plots for $10/3$ and $11/3$ FQHS diverge (Fig. 3(e)), indicating the breaking of PHS around half-filling. At $B = 12$ T, the $7/2$ state is well-formed, the odd-denominator Jain states $\nu = 10/3$ and $\nu = 17/5$ survive, while their hole-conjugate states $\nu = 11/3$ and $\nu = 18/5$ states completely disappear [see Fig. 3(c) and (f)].

Fig. 3(g) compares the dependence of Δ_ν on B for $\nu = 7/2$ (left y-axis) and $\nu = 10/3$, and $11/3$ (right y-axis). For $B \leq 7.5$ T (orange shaded region), $\Delta_{7/2} = 0$, and $\Delta_{10/3} = \Delta_{11/3}$, demonstrating perfect particle-hole symmetry in the absence of an incompressible state at half-filling. At intermediate values of B (yellow shaded region), the $\nu = 7/2$ state begins to develop, and particle-hole symmetry is broken as evidenced by $\Delta_{10/3} \neq \Delta_{11/3}$. At large magnetic fields ($B \geq 10$ T, gray shaded region), the $\Delta_{7/2}$ stabilizes, simultaneously $\Delta_{11/3}$ goes to zero, establishing a complete lifting of the PHS in the presence of even-denominator FQHS.

III. DISCUSSION

Recent studies have reported the observation of even-denominator fractional quantum Hall states (FQHS) at $\nu = -3/2$, $\nu = 3/2$, $\nu = 9/2$, and $\nu = -9/2$ in ABA-trilayer graphene [64], occurring within the $N = 1$ orbital. Notably, our detection of the $\nu = 7/2$ and $\nu = 5/2$ states within

the $N = 0$ orbital of the monolayer sector presents a distinct scenario where LL mixing is likely important. Owing to the $SU(4)$ symmetry of the long-range Coulomb interaction in graphene, LL mixing usually occurs only between levels of different orbitals [44]. However, in the present case, even-denominator FQHSs arise from LL mixing between two $N = 0$ levels, which differ in their valley index, with identical spins at $\nu = 5/2$ and opposite spins at $\nu = 7/2$. To understand this, it is crucial to account for the lattice-scale corrections [65, 66] to the long-range Coulomb interaction in TLG. Fig. 4 compares the wavefunctions of single-layer, bilayer, and Bernal trilayer graphene. The wavefunctions in the $N = 0$ LLs of monolayer and bilayer graphene are invariant under the inversion operation \mathcal{I} [see Fig. 4(a–b)]. Consequently, the wavefunctions in the two valleys (denoted by $+$ and $-$) are identical, differing only by an exchange of the sublattice and layer indices leading to symmetry under the inversion operator \mathcal{I} on the crystal. In contrast, ABA TLG lacks inversion symmetry, and that appears to be crucial here since experiments probing the same regime of the crossing of two $N=0$ LLs in BLG did not find any signatures of incompressibility at half-filling [28]. Also, aside from a single report [67], even-denominator FQHSs have not been observed in the half-filled $N=0$ LLs of MLG [68].

The lack of inversion symmetry in TLG distinguishes the two valleys in the $N = 0$ LL [see Fig. 4(c)]. The difference in the local charge environment between the $|0, +\rangle$ and $|0, -\rangle$ states can give rise to additional isospin-dependent interactions that are absent in monolayer and bilayer graphene. We posit that under the influence of all these lattice terms, the bands with different valleys hybridize, breaking the usual valley-spin symmetries and opening a gap at the crossing points, modifying the effective intra-LL interaction. Generically, the LL mixing induced by these couplings within the $N = 0$ orbital is not expected to significantly affect the Coulomb interaction because lattice-scale couplings are typically much weaker than the Coulomb scale. However, when two LLs are very close in energy, the LL mixing induced by these couplings can get enhanced, leading to a suppression of the short-range part of the interaction that stabilizes even-denominator FQH phases over the CFFL. Further theoretical studies are essential to verify this proposed scenario.

IV. DATA AVAILABILITY

The authors declare that the data supporting the findings of this study are available within the main text and its Supplementary Information. Other relevant data are available from the corre-

sponding author upon request.

V. CODE AVAILABILITY

The codes that support the findings of this study are available from the corresponding author upon request.

VI. METHODS

Devices based on dual-graphite-gated ABA-TLG heterostructures were fabricated using a dry transfer technique. Electron beam lithography was employed to define the device geometry, followed by reactive ion etching (RIE) to pattern the graphene layers. Cr/Pd/Au contacts were thermally evaporated onto the patterned device. All measurements were performed in a dilution refrigerator with a base temperature of 20 mK using a standard low-frequency AC method at 11 Hz.

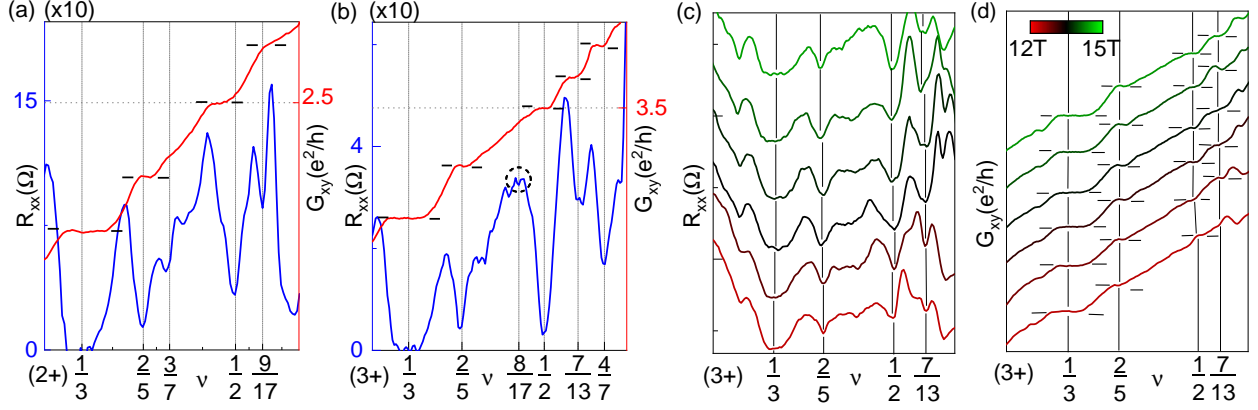


FIG. 1. Even- and odd-denominator FQHSs in ABA Trilayer graphene (between $\nu = 2$ to $\nu = 3$ and $\nu = 3$ to $\nu = 4$). Longitudinal resistance R_{xx} (left-axis; solid blue line) and hall conductance G_{xy} (right-axis; solid red line) as a function of filling factor ν for (a) $\nu = 2$ to $\nu = 3$ measured at $B = 12$ T and $D = -0.1$ V/nm, and (b) $\nu = 3$ to $\nu = 4$ measured at $B = 15$ T and $D = -0.08$ V/nm. (c) R_{xx} and (d) G_{xy} as a function of ν in the vicinity of $\nu = 7/2$ for representative values of B , at a fixed $D = -0.785$ V/nm. All data were acquired at $T = 20$ mK.

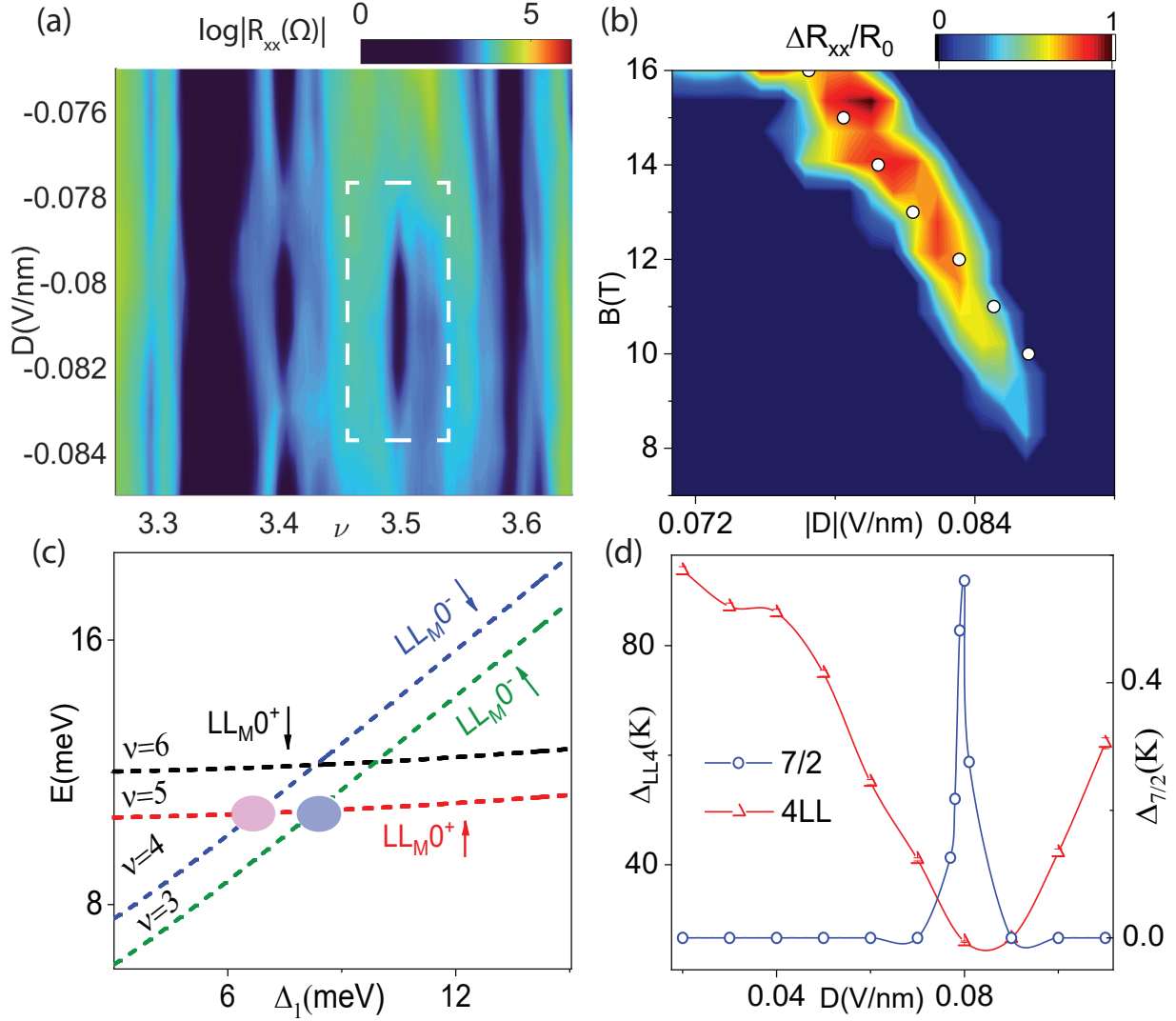


FIG. 2. **D -dependence of the even-denominator FQHS** (a) Contour plot of R_{xx} in the $\nu - D$ plane; the data were acquired at $B = 12$ T and $T = 20$ mK over the filling factor range $\nu = 3$ to $\nu = 4$ (b) Plot of $\Delta R_{xx}/R_0$ versus B and D . The filled white circles are the calculated crossing points between $LL_M^{0+} \uparrow$ and $LL_M^{0-} \downarrow$ LLs. (c) Simulated LL spectrum of ABA trilayer graphene as a function of energy E and interlayer potential Δ_1 . The $\nu = 7/2$ FQHS appears in the region marked by the red ellipse, while the $\nu = 5/2$ appears in the region marked by the blue ellipse. (d) Measured activation gaps of $\nu = 7/2$ (blue open circles; right y-axis) and $\nu = 4$ (red open circles, left y-axis) as a function of D ; the data were acquired at $B = 13$ T. The lines are a guide to the eye.

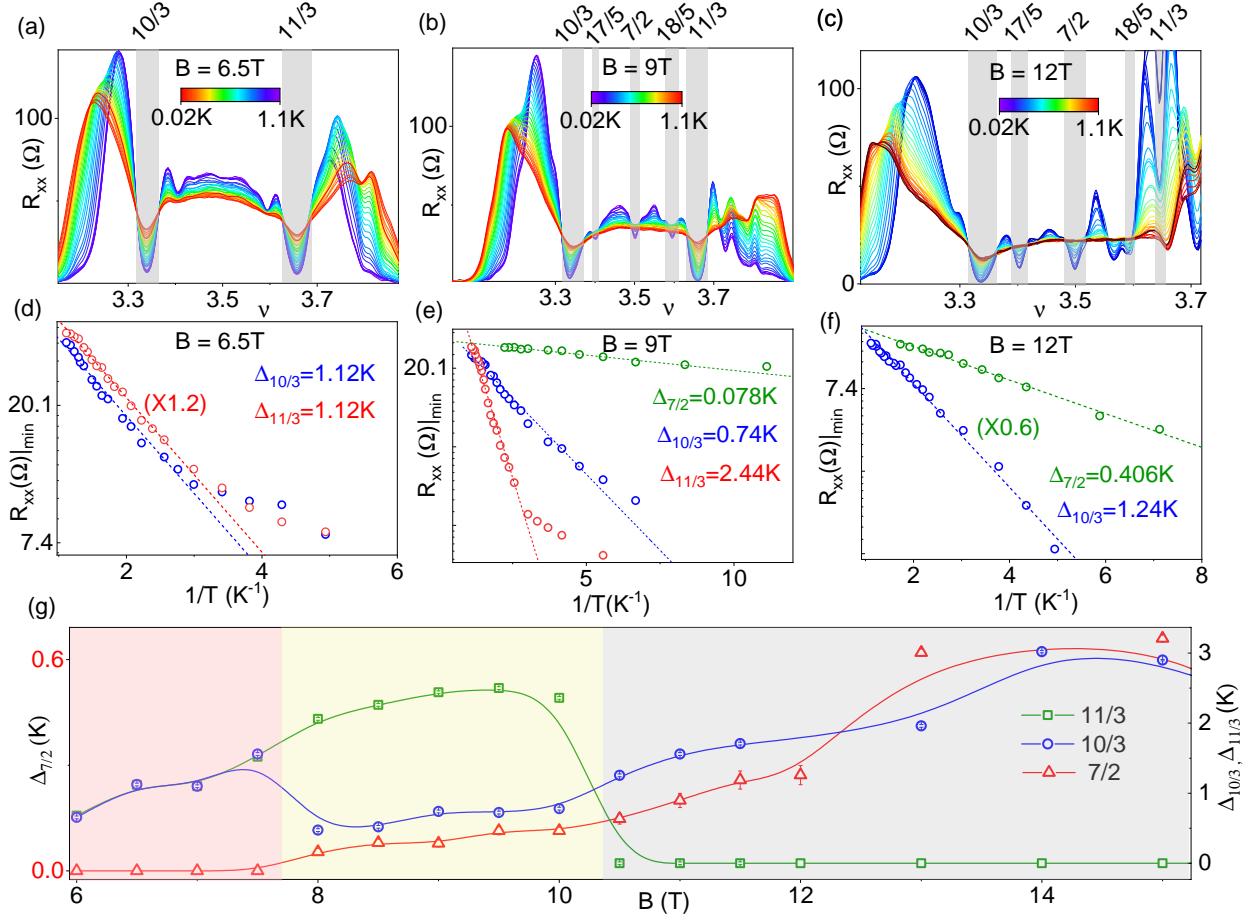


FIG. 3. **Activation gaps of even and odd denominator FQHS.** (a-c) Plots of R_{xx} versus ν at various representative temperatures T for $D = -0.08$ V/nm, covering the range between $\nu = 3$ and $\nu = 4$ at magnetic fields of (a) $B = 6.5$ T, (b) $B = 9$ T, and (c) $B = 12$ T. (d-f) Minimum values of R_{xx} versus $1/T$ for different FQHS within the same ν range for (d) $B = 6.5$ T, (e) $B = 9$ T, and (f) $B = 12$ T. The open symbols represent experimental data, while the dashed lines correspond to Arrhenius fits. (g) Energy gap as a function of the magnetic field B for $\nu = 7/2$, $\nu = 11/3$, and $\nu = 10/3$. The orange-shaded region indicates the particle-hole symmetric regime, where the gap at $\nu = 7/2$ is zero. The $7/2$ FQHS emerges in the yellow-shaded region, and particle-hole symmetry breaks down. The gray-shaded region highlights the high- B range where $\Delta_{7/2}$ becomes large, and the gap at $\Delta_{11/3}$ vanishes. The lines are guides to the eye.

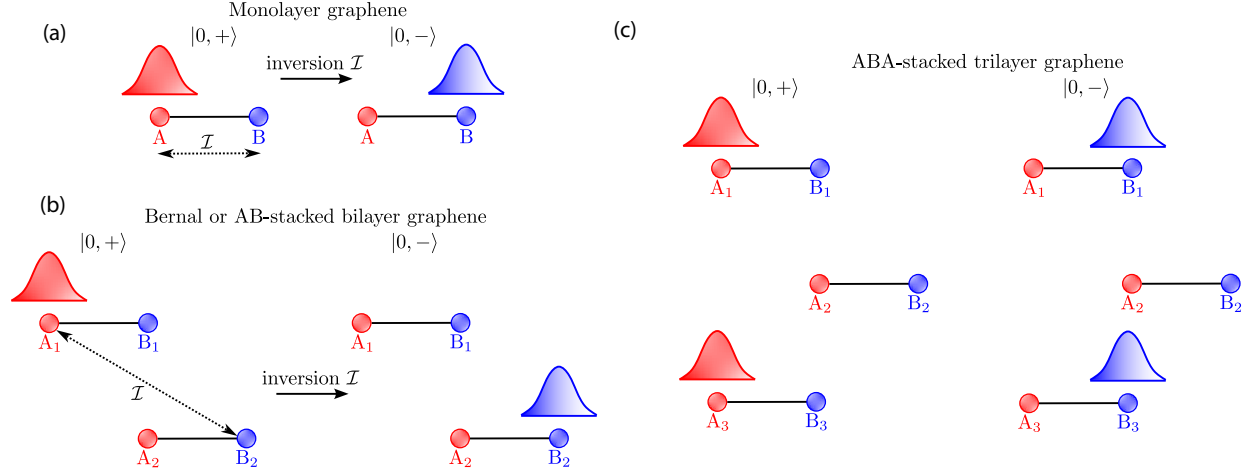


FIG. 4. **Inversion symmetry in graphene.** (a) and (b) Schematics of the wavefunctions in the $N = 0$ LLs of monolayer and bilayer graphene, respectively, which are invariant under the inversion operation \mathcal{I} . The wavefunctions in the two valleys are denoted by $+$ and $-$. (c) Schematic of the wavefunctions in ABA-trilayer graphene for the two valleys. The absence of inversion symmetry in ABA-trilayer graphene is evident from the distinct local charge environments of the $|0, +\rangle$ and $|0, -\rangle$ states.

VII. ACKNOWLEDGEMENTS

A. C. B. thanks the Science and Engineering Research Board (SERB) of the Department of Science and Technology (DST) for financial support through the Mathematical Research Impact Centric Support (MATRICS) Grant No. MTR/2023/000002. A.B. acknowledges funding from U.S. Army DEVCOM Indo-Pacific (Project number: FA5209 22P0166) and Department of Science and Technology, Govt of India (DST/SJF/PSA-01/2016-17). K.W. and T.T. acknowledge support from the JSPS KAKENHI (Grant Numbers 21H05233 and 23H02052) and World Premier International Research Center Initiative (WPI), MEXT, Japan.

AUTHOR CONTRIBUTIONS

T.C., S.K., and A.B. conceived the idea of the study, conducted the measurements, and analyzed the results. T.T. and K.W. provided the hBN crystals. H.S., M.J., A.C.B., and U.K. developed the theoretical model. All the authors contributed to preparing the manuscript.

[†] These authors contributed equally.

COMPETING INTERESTS

The authors declare no competing interests.

SUPPLEMENTARY INFORMATION

SUPPLEMENTARY NOTE 1: DEVICE FABRICATION AND CHARACTERIZATION.

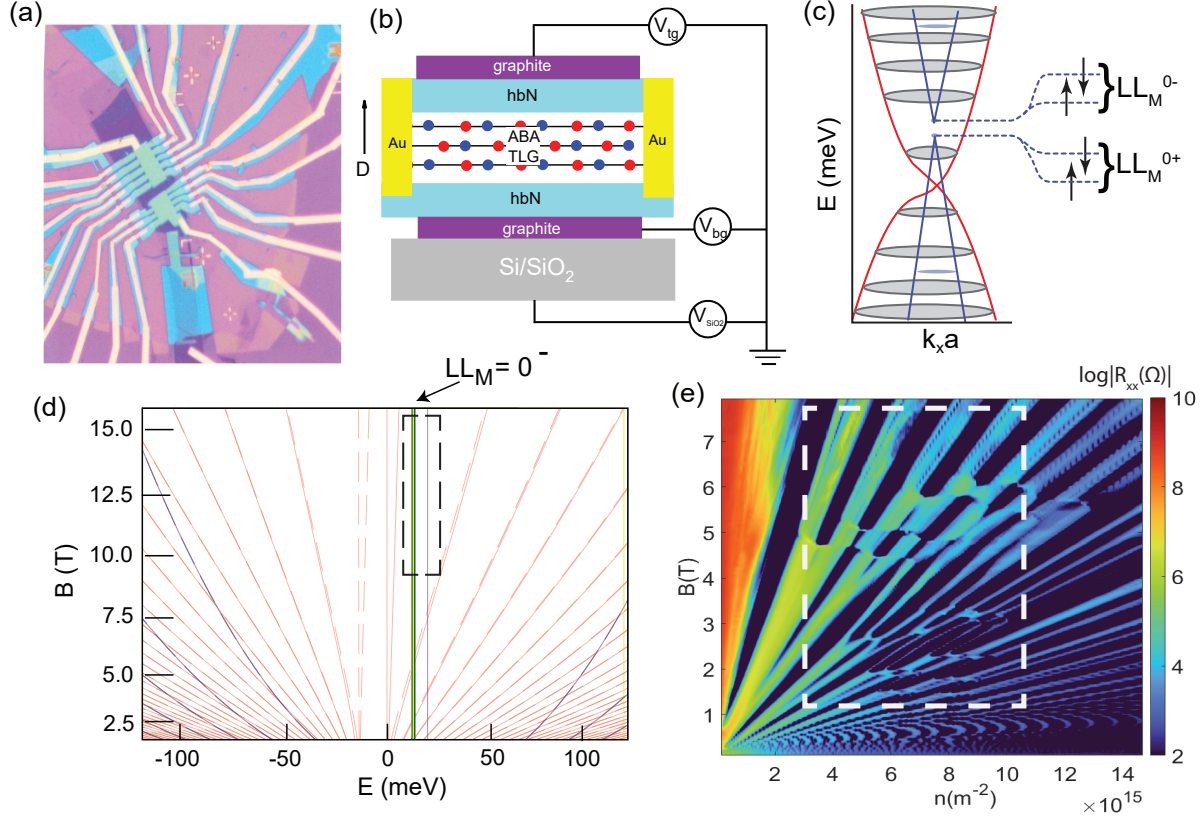


FIG. Supplementary Figure 1. Device Schematics and characterization. (a) Optical image of the device. (b) Device schematic showing the various gate configurations used in the measurements. The top and bottom gates were used to control the vertical displacement field D and the carrier density n across the sample with SiO₂/Si back gate used to dope the contacts. (c) Calculated band structure of Bernal-stacked trilayer graphene at $D = 0$ V/nm. The dashed line marks the $N = 0$ LLs of the MLL band, the focus of this study. (d) Calculated LL spectrum as a function of energy E and magnetic field B for $D = 0$ V/nm. The blue lines are the MLL LLs, while the red lines are the BLL LLs. Solid and dotted lines mark the LLs from the K and K' -valleys. The solid green line marks the $LL_M^{0-} \uparrow$ and $LL_M^{0-} \downarrow$ monolayer-like LLs, which host the fractional quantum Hall (FQH) states probed in this study. (e) Contour plot of R_{xx} in log scale as a function of number density and magnetic field at $D = 0$ V/nm. A dashed rectangle marks the crossing of LL_M^0 LL of the MLL band with BLL LLs, corresponding to the calculated LL plot in (d).

Bernal-stacked trilayer graphene (TLG), hBN, and graphite flakes are mechanically exfoli-

ated on 280 nm thick SiO₂ substrate. We used optical contrast and Raman spectroscopy [69, 70] to identify ABA TLG flakes. We have fabricated heterostructure using the standard dry pickup and transfer technique. We defined 1-D metallic contacts on the heterostructure using e-beam lithography followed by reactive ion etching using CHF₃/O₂ gas and Cr/Pd/Au thermal deposition [55, 71]. The device was then etched into a Hall bar shape (**Supplementary Figure 1(a)**). To prevent the formation of p-n junctions, we dope the graphene contacts extended out of the device using SiO₂/Si back gate.

A device schematic with different gate configurations is shown in **Supplementary Figure 1(b)**. We used a dual-gate configuration to tune the vertical displacement field $D = [(C_{bg}V_{bg} - C_{tg}V_{tg})/2\epsilon_0]$ and carrier density $n = [(C_{bg}V_{bg} + C_{tg}V_{tg})/e]$ across the sample independently. Here, C_{bg} and C_{tg} represent the back-gate and top-gate capacitance, respectively. V_{bg} and V_{tg} are the back-gate and top-gate voltages. The gate capacitance is estimated from quantum Hall measurements.

Supplementary Figure 1(c) shows the calculated band structure of ABA TLG at $D = 0$ V/nm. It can be decomposed into two independent sectors – a linearly dispersing monolayer-like (MLL) band (blue solid line) and a massive bilayer-like (BLL) band (red solid line). Dashed lines mark the $LL_M^{0\pm}$ LLs formed in the MLL band at a finite perpendicular magnetic field B . Here 0 is the orbital index, and \pm is the valley index of the LL. In this study, we have focused on LL_M^{0+} LL. The LLs arising from the BLL band are shown as gray ellipses.

Supplementary Figure 1(d) shows the simulated LL spectrum as a function of energy and magnetic field at $D = 0$ V/nm. Here, red lines mark the LLs from the BLL band, and blue lines mark the LLs from the MLL band. The green solid line highlights the crossing of LL_M^{0-} LL of the MLL band with several BLL LLs. **Supplementary Figure 1(e)** shows the contour plot of R_{xx} as a function of magnetic field and number density. The dashed rectangle marks the crossing region of LL_M^0 LL of the MLL band with multiple BLL LLs, confirming the system to be ABA trilayer graphene.

SUPPLEMENTARY NOTE 2: EVOLUTION OF DAUGHTER STATES WITH DISPLACEMENT FIELD.

Supplementary Figure 2(a) and **Supplementary Figure 2(b)** show the line plots of R_{xx} versus ν for different values of D in the vicinity of $\nu = 2 + 1/2$ and $\nu = 3 + 1/2$, measured at $B = 12$ T.

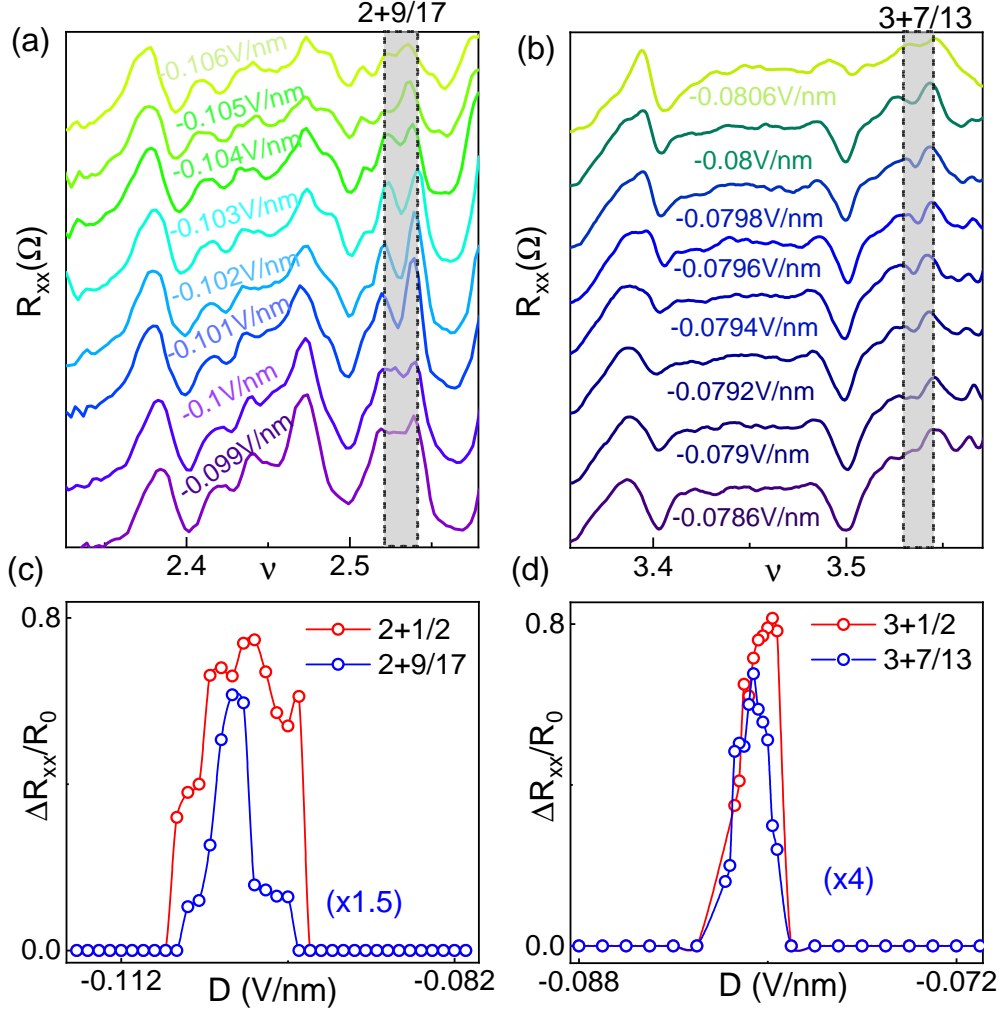


FIG. **Supplementary Figure 2. Evolution of daughter states with displacement field.** Plot of R_{xx} as a function of ν at different values of D in the vicinity of (a) $\nu = 2 + 1/2$, and (b). The data is taken at $B = 12$ T. The Shaded region marks the behavior of daughter states with D . (c) and (d) plots of normalized dip ($\Delta R_{xx}/R_0$) as a function of D at $\nu = 2 + 1/2, 2 + 9/17$ and $\nu = 3 + 1/2, 3 + 7/13$ respectively.

The shaded region marks the evolution of daughter states at $\nu = 2 + 9/17$ and $\nu = 3 + 7/13$ with D . Minima of R_{xx} at these fraction fillings survives over a narrow range of D : $0.097 < |D| < 0.105$ V/nm for $\nu = 2 + 9/17$ and $0.078 < |D| < 0.081$ V/nm for $\nu = 3 + 7/13$. It vanishes beyond this range of D .

To confirm these observations, we calculated normalized dips in the longitudinal resistance, $\Delta R_{xx}/R_0$, (see Supplementary Note 4) for even-denominator states at $\nu = 2 + 1/2, 3 + 1/2$ and their corresponding daughter states at $\nu = 2 + 9/17, 3 + 7/13$. **Supplementary Figure 2(c)** and **Supplementary Figure 2(d)** show the plots of $\Delta R_{xx}/R_0$ as a function of D for FQHs at $\nu =$

$2 + 1/2$, $2 + 9/17$ and $\nu = 3 + 1/2$, $3 + 7/13$ respectively. These plots establish that the daughter state at $3 + 7/13$ ($2 + 9/17$) appears over the exact same range of D as the even-denominator FQHS $\nu = 7/2$ ($\nu = 5/2$).

SUPPLEMENTARY NOTE 3: DEPENDENCE OF $\nu = 2 + 1/2$ ON D .

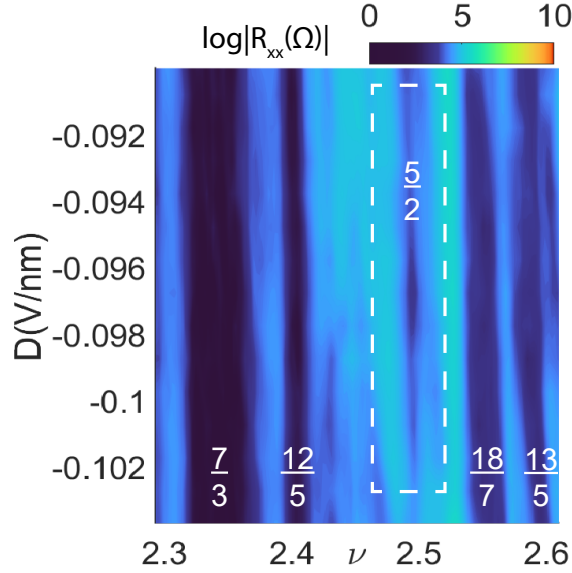


FIG. **Supplementary Figure 3. Evolution of $\nu = 2 + 1/2$ state with D .** Contour plot of R_{xx} as a function of ν and D measured at $B = 12$ T. Here, dashed rectangle marks the region where $\nu = 2 + 1/2$ state is formed.

Supplementary Figure 3 shows the contour plot of R_{xx} as a function of ν and D measured at $B = 12$ T. The dark region corresponds to R_{xx} minima at various fractional fillings marked in the plot. The dashed rectangle highlights the evolution of $\nu = 2 + 1/2$ state with D . Notably, $\nu = 2 + 1/2$ remains robust over the range $0.092 < |D| < 0.1$ V/nm.

Comparing it with the simulated plot in Fig 2(c) of the main manuscript, we observe that the crossing responsible for the emergence of $\nu = 2 + 1/2$ state occurs between $LL_M^{0-} \uparrow$ and $LL_M^{0+} \uparrow LL$ at crossing value of $\Delta_1 = 8.29$ meV. This is in good agreement with the experimental $|D|$ values, using the conversion factor $\Delta_1 = -[(d_{\perp}/2\epsilon_{TLG}) \times D]e$ [72], which leads to $\Delta_1(\text{meV}) = 85 D$ (V/nm). Here, $d_{\perp} = 0.67$ nm is the separation between top and bottom layers of TLG, ϵ_{TLG} is the dielectric constant of the TLG, e is the electronic charge.

This conversion factor also aligns with the observed D range ($0.079 < |D| < 0.083$ V/nm) for

$\nu = 3 + 1/2$ state, corresponding to $\Delta_1 = 6.7$ meV. This value matches well with the crossing point between $LL_M^{0-} \downarrow$ and $LL_M^{0+} \uparrow$ LL of Fig 2(c) of the main manuscript. This further confirms that the origin of even denominator FQHs lies in the Landau level crossings of LL_M^0 LL from the monolayer-like band.

SUPPLEMENTARY NOTE 4: DEFINITION OF $\Delta R_{xx}/R_0$

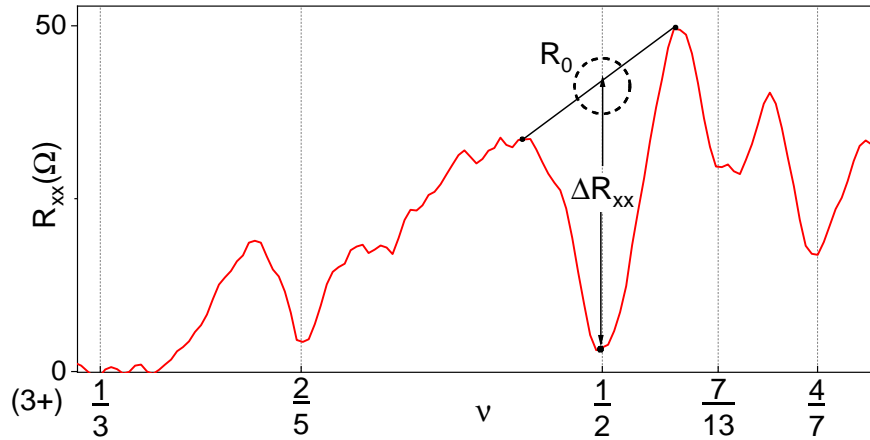


FIG. **Supplementary Figure 4.** Line plot of R_{xx} as a function of ν . Here, $\Delta R_{xx}/R_0$ defines the normalized dip of the even denominator FQHS.

Supplementary Figure 4 shows the line scan of R_{xx} as a function of filling factor ν in the vicinity of $\nu = 3 + 1/2$ state. This plot illustrates the method used to calculate the normalized dip of even-denominator FQHS ($\Delta R_{xx}/R_0$), which is then used to construct Fig 2(b) of the main manuscript and **Supplementary Figure 2(c-d)** of this document.

SUPPLEMENTARY NOTE 5: ENERGY GAP OF THE 4th LL

Supplementary Figure 5(a) shows the plot of R_{xx} as a function of ν at different temperatures measured at $B = 13$ T and $|D| = 0.1$ V/nm in the vicinity of $LL = 4$. Arrhenius fits to data points obtained from the minima of R_{xx} at various D is shown in **Supplementary Figure 5(b)**. From the slopes of these fits, we extract the values of Δ using **Supplementary Equation 1**.

$$R_{xx} = R_0 \exp(-\Delta/2k_B T). \quad (\text{Supplementary Equation 1})$$

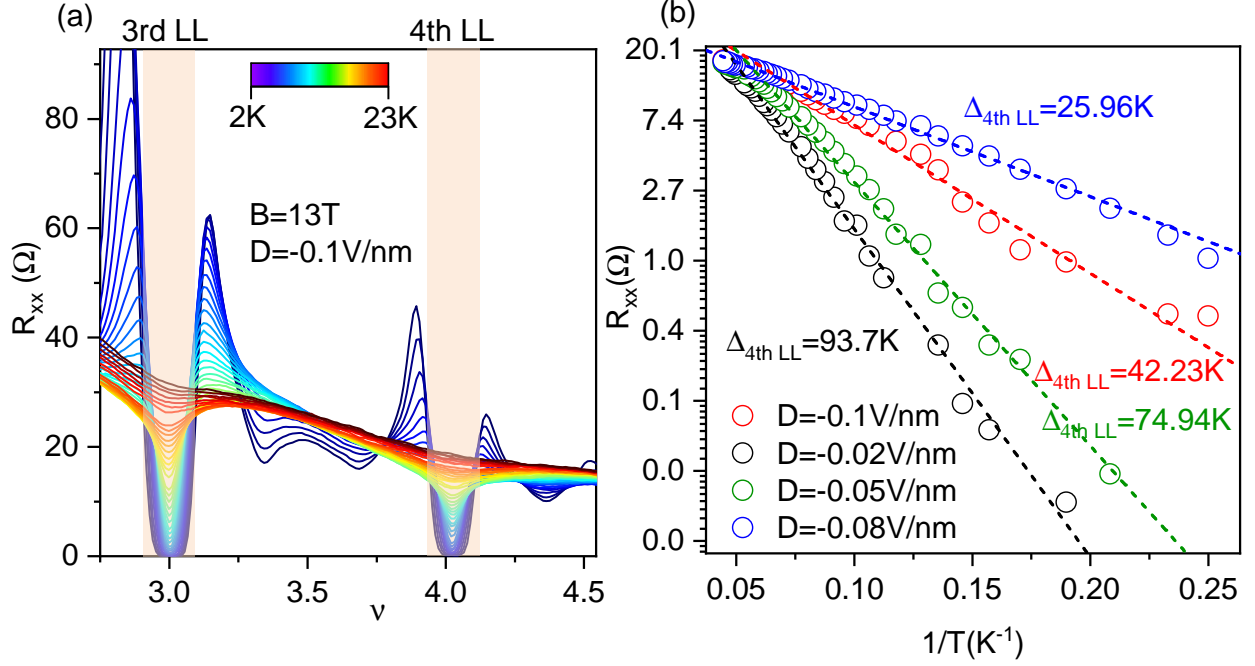


FIG. **Supplementary Figure 5. Activation gaps of the fourth LL.** (a) Line plots of R_{xx} as a function of ν at various temperatures (2 K to 23 K), measured at $B = 13$ T and $|D| = 0.1$ V/nm. (b) Arrhenius fits to R_{xx} at $|D| = -0.1$ V/nm, $|D| = 0.02$ V/nm, $|D| = 0.0$ V/nm and $|D| = 0.08$ V/nm.

SUPPLEMENTARY NOTE 6: DETAILS OF SIMULATIONS.

We have calculated the Landau spectrum at $B = 12$ T using the tight-binding model based on the Slonczewski-Weiss-McClure parametrization of tight binding model [49, 64, 73]. This model consist of six parameters $\{\gamma_0, \gamma_1, \dots, \gamma_5\}$, which represent hopping from

$$A_i \leftrightarrow B_i : \gamma_0, B_{1/3} \leftrightarrow A_2 : \gamma_1 \quad (\text{Supplementary Equation 2a})$$

$$A_1 \leftrightarrow A_3 : \frac{1}{2}\gamma_2, A_{1/3} \leftrightarrow B_2 : \gamma_3 \quad (\text{Supplementary Equation 2b})$$

$$(A/B)_{1/3} \leftrightarrow (A/B)_2 : -\gamma_4, B_1 \leftrightarrow B_3 : \frac{1}{2}\gamma_5 \quad (\text{Supplementary Equation 2c})$$

where A(B) represents sublattice and index i represents layer $1 \dots 3$. There is an additional parameter δ which is there to take the on-site potential for sites on top of each other (B_1 , B_3 , and A_2) into

account. Hamiltonian of this system in basis $\{A_1, B_1, A_2, B_2, A_3, B_3\}$ can be written as

$$H_0 = \begin{pmatrix} 0 & \gamma_0 t_{\mathbf{k}}^* & \gamma_4 t_{\mathbf{k}}^* & \gamma_3 t_{\mathbf{k}} & \gamma_2/2 & 0 \\ \gamma_0 t_{\mathbf{k}} & \delta & \gamma_1 & \gamma_4 t_{\mathbf{k}}^* & 0 & \gamma_5/2 \\ \gamma_4 t_{\mathbf{k}} & \gamma_1 & \delta & \gamma_0 t_{\mathbf{k}}^* & \gamma_4 t_{\mathbf{k}} & \gamma_1 \\ \gamma_3 t_{\mathbf{k}}^* & \gamma_4 t_{\mathbf{k}} & \gamma_0 t_{\mathbf{k}} & 0 & \gamma_3 t_{\mathbf{k}}^* & \gamma_4 t_{\mathbf{k}} \\ \gamma_2/2 & 0 & \gamma_4 t_{\mathbf{k}}^* & \gamma_3 t_{\mathbf{k}} & 0 & \gamma_0 t_{\mathbf{k}}^* \\ 0 & \gamma_5/2 & \gamma_1 & \gamma_4 t_{\mathbf{k}}^* & \gamma_0 t_{\mathbf{k}} & \delta \end{pmatrix} \quad (\text{Supplementary Equation 3})$$

where $t_{\mathbf{k}} = \sum_{j=1}^3 e^{i\mathbf{k}\cdot\mathbf{a}_j}$, $\mathbf{a}_0 = a(0, 1/\sqrt{3})$, $\mathbf{a}_{1/2} = a(\mp 1/2, -1/2\sqrt{3})$ and $a=2.46 \text{ \AA}$. Effective low energy Hamiltonian can be constructed by expanding the above Hamiltonian near K^+/K^- points. Low energy Hamiltonian can then be written simply by substituting $\gamma_i t_{\mathbf{k}} \rightarrow v_i \pi$, where

$$\pi = \xi k_x + i k_y \quad (\text{Supplementary Equation 4a})$$

$$\hbar v_i = \frac{\sqrt{3}}{2} a \gamma_i \quad (\text{Supplementary Equation 4b})$$

electric field can be taken into account by introducing onsite potential for each layer $V_1 \dots V_3$. Where effect of external and intrinsic electric field can be described by parameters Δ_1 and Δ_2 respectively.

$$\Delta_1 = (-e) \frac{V_1 - V_2}{2}, \Delta_2 = (-e) \frac{V_1 + V_3 - 2V_2}{6} \quad (\text{Supplementary Equation 5})$$

Without external electric field, Hamiltonian contains monolayer-like and bilayer-like bands completely uncoupled from each other. This can be easily seen if one shifts to basis

$\left\{ \frac{A_1 - A_3}{\sqrt{2}}, \frac{B_1 - B_3}{\sqrt{2}}, \frac{A_1 + A_3}{\sqrt{2}}, B_2, A_2, \frac{B_1 + B_3}{\sqrt{2}} \right\}$, where Hamiltonian takes form

$$H_0 + H_{\Delta_2} = \begin{pmatrix} H_{slg} & 0 \\ 0 & H_{blg} \end{pmatrix} \quad (\text{Supplementary Equation 6})$$

and external electric field couples both the blocks.

$$H_{\Delta_1} = \begin{pmatrix} 0 & H_{ext} \\ H_{ext} & 0 \end{pmatrix}, H_{ext} = \begin{pmatrix} \Delta_1 & 0 & 0 & 0 \\ 0 & 0 & 0 & \Delta_1 \end{pmatrix} \quad (\text{Supplementary Equation 7})$$

where

$$H_{slg} = \begin{pmatrix} \Delta_2 - \gamma_2/2 & v_0 \pi^\dagger \\ v_0 \pi & -\gamma_5/2 + \delta + \Delta_2 \end{pmatrix} \quad (\text{Supplementary Equation 8})$$

and

$$H_{blg} = \begin{pmatrix} \gamma_2/2 + \delta & \sqrt{2}v_3\pi & -\sqrt{2}v_4\pi^\dagger & v_0\pi^\dagger \\ \sqrt{2}v_3\pi^\dagger & -2\Delta_2 & v_0\pi & -\sqrt{2}v_4\pi \\ -\sqrt{2}v_4\pi & v_0\pi^\dagger & \delta - 2\Delta_2 & \sqrt{2}\gamma_1 \\ v_0\pi & -\sqrt{2}v_4\pi^\dagger & \sqrt{2}\gamma_1 & \gamma_5/2 + \delta + \Delta_2 \end{pmatrix} \quad (\text{Supplementary Equation 9})$$

the following parameters: $\gamma_0 = 3.1$ eV, $\gamma_1 = 0.39$ eV, $\gamma_2 = -0.005$ eV, $\gamma_3 = 0.275$ eV, $\gamma_4 = 0.040$ eV, $\gamma_5 = 0.005$ eV, $\delta = 0.0108$ eV, and $\Delta_2 = 0.003$ eV. For calculation of Landau Level spectra, we make following substitution

$$\pi \rightarrow \pi - e(A_x + iA_y) \quad (\text{Supplementary Equation 10})$$

We then choose landau gauge, where $A_x = 0, A_y = Bx$. As there is no y dependence in Hamiltonian, k_y is conserved and one can see that π operators take the form

$$\pi = \frac{-i\hbar}{l_B}(\xi\partial_x + x - k_y) \quad (\text{Supplementary Equation 11})$$

One can see, in Landau level basis at particular value of k_y , this operator act as raising/lowering operator.

$$K_+ : \pi|n\rangle = \frac{i\hbar}{l_B} \sqrt{2(n+1)}|n+1\rangle \quad (\text{Supplementary Equation 12a})$$

$$K_+ : \pi^\dagger|n\rangle = -\frac{i\hbar}{l_B} \sqrt{2n}|n-1\rangle \quad (\text{Supplementary Equation 12b})$$

$$K_- : \pi|n\rangle = \frac{i\hbar}{l_B} \sqrt{2n}|n-1\rangle \quad (\text{Supplementary Equation 12c})$$

$$K_- : \pi^\dagger|n\rangle = -\frac{i\hbar}{l_B} \sqrt{2(n+1)}|n+1\rangle \quad (\text{Supplementary Equation 12d})$$

We then choose a cutoff for Landau Level basis α . Thus π operators are then replaced by $\alpha \times \alpha$ matrices. Choosing a finite cutoff will give rise to un-physical eigenvalues in low energy region. These eigenvalues can be removed by filtering the eigenvalues which have large $|n\rangle$ contribution. For our calculations, we choose $\alpha = 100$.

-
- [1] R. B. Laughlin, *Phys. Rev. Lett.* **50**, 1395 (1983).
- [2] D. C. Tsui, H. L. Stormer, and A. C. Gossard, *Phys. Rev. Lett.* **48**, 1559 (1982).
- [3] Z. Papić and A. C. Balram, *Fractional quantum hall effect in semiconductor systems* (2022), [arXiv:2205.03421 \[cond-mat.mes-hall\]](https://arxiv.org/abs/2205.03421).
- [4] D. Arovas, J. R. Schrieffer, and F. Wilczek, *Phys. Rev. Lett.* **53**, 722 (1984).
- [5] B. I. Halperin, *Phys. Rev. Lett.* **52**, 1583 (1984).
- [6] G. Moore and N. Read, *Nuclear Physics B* **360**, 362 (1991).
- [7] D. E. Feldman and B. I. Halperin, *Reports on Progress in Physics* **84**, 076501 (2021).
- [8] H. Bartolomei, M. Kumar, R. Bisognin, A. Marguerite, J.-M. Berroir, E. Bocquillon, B. Plaçais, A. Cavanna, Q. Dong, U. Gennser, Y. Jin, and G. Fève, *Science* **368**, 173 (2020), <https://www.science.org/doi/pdf/10.1126/science.aaz5601>.
- [9] H. K. Kundu, S. Biswas, N. Ofek, V. Umansky, and M. Heiblum, *Nature Physics* **19**, 515 (2023).
- [10] J. Nakamura, S. Liang, G. C. Gardner, and M. J. Manfra, *Nature Physics* **16**, 931 (2020).
- [11] S. Das Sarma, M. Freedman, and C. Nayak, *Phys. Rev. Lett.* **94**, 166802 (2005).
- [12] C. Nayak, S. H. Simon, A. Stern, M. Freedman, and S. Das Sarma, *Rev. Mod. Phys.* **80**, 1083 (2008).
- [13] R. L. Willett, K. Shtengel, C. Nayak, L. N. Pfeiffer, Y. J. Chung, M. L. Peabody, K. W. Baldwin, and K. W. West, *Phys. Rev. X* **13**, 011028 (2023).
- [14] X. Lin, R. Du, and X. Xie, *National Science Review* **1**, 564 (2014), <https://academic.oup.com/nsr/article-pdf/1/4/564/31568876/nwu071.pdf>.
- [15] M. Banerjee, M. Heiblum, V. Umansky, D. E. Feldman, Y. Oreg, and A. Stern, *Nature* **559**, 205 (2018).
- [16] B. Dutta, V. Umansky, M. Banerjee, and M. Heiblum, *Science* **377**, 1198 (2022), <https://www.science.org/doi/pdf/10.1126/science.abm6571>.
- [17] W. Pan, J.-S. Xia, V. Shvarts, D. E. Adams, H. L. Stormer, D. C. Tsui, L. N. Pfeiffer, K. W. Baldwin, and K. W. West, *Phys. Rev. Lett.* **83**, 3530 (1999).
- [18] J. P. Eisenstein, K. B. Cooper, L. N. Pfeiffer, and K. W. West, *Phys. Rev. Lett.* **88**, 076801 (2002).
- [19] Y. Liu, J. Shabani, D. Kamburov, M. Shayegan, L. N. Pfeiffer, K. W. West, and K. W. Baldwin, *Phys. Rev. Lett.* **107**, 266802 (2011).
- [20] Y. W. Suen, L. W. Engel, M. B. Santos, M. Shayegan, and D. C. Tsui, *Phys. Rev. Lett.* **68**, 1379 (1992).

- [21] R. Willett, J. P. Eisenstein, H. L. Störmer, D. C. Tsui, A. C. Gossard, and J. H. English, [Phys. Rev. Lett. **59**, 1776 \(1987\)](#).
- [22] J. P. Eisenstein, G. S. Boebinger, L. N. Pfeiffer, K. W. West, and S. He, [Phys. Rev. Lett. **68**, 1383 \(1992\)](#).
- [23] J. Falson, D. Maryenko, B. Friess, D. Zhang, Y. Kozuka, A. Tsukazaki, J. H. Smet, and M. Kawasaki, [Nature Physics **11**, 347 \(2015\)](#).
- [24] J. Falson, D. Tabrea, D. Zhang, I. Sodemann, Y. Kozuka, A. Tsukazaki, M. Kawasaki, K. von Klitzing, and J. H. Smet, [Science Advances **4**, eaat8742 \(2018\)](#), <https://www.science.org/doi/pdf/10.1126/sciadv.aat8742>.
- [25] J. I. A. Li, C. Tan, S. Chen, Y. Zeng, T. Taniguchi, K. Watanabe, J. Hone, and C. R. Dean, [Science **358**, 648 \(2017\)](#), <https://www.science.org/doi/pdf/10.1126/science.aa02521>.
- [26] A. A. Zibrov, C. Kometter, H. Zhou, E. M. Spanton, T. Taniguchi, K. Watanabe, M. P. Zaletel, and A. F. Young, [Nature **549**, 360 \(2017\)](#).
- [27] Y. Kim, A. C. Balram, T. Taniguchi, K. Watanabe, J. K. Jain, and J. H. Smet, [Nature Physics **15**, 154 \(2019\)](#).
- [28] K. Huang, H. Fu, D. R. Hickey, N. Alem, X. Lin, K. Watanabe, T. Taniguchi, and J. Zhu, [Phys. Rev. X **12**, 031019 \(2022\)](#).
- [29] A. C. Balram, [Phys. Rev. B **105**, L121406 \(2022\)](#).
- [30] M. S. Hossain, M. K. Ma, Y. J. Chung, S. K. Singh, A. Gupta, K. W. West, K. W. Baldwin, L. N. Pfeiffer, R. Winkler, and M. Shayegan, [Phys. Rev. Lett. **130**, 126301 \(2023\)](#).
- [31] A. Assouline, T. Wang, H. Zhou, L. A. Cohen, F. Yang, R. Zhang, T. Taniguchi, K. Watanabe, R. S. K. Mong, M. P. Zaletel, and A. F. Young, [Phys. Rev. Lett. **132**, 046603 \(2024\)](#).
- [32] M. S. Hossain, M. K. Ma, Y. J. Chung, L. N. Pfeiffer, K. W. West, K. W. Baldwin, and M. Shayegan, [Phys. Rev. Lett. **121**, 256601 \(2018\)](#).
- [33] Q. Shi, E.-M. Shih, M. V. Gustafsson, D. A. Rhodes, B. Kim, K. Watanabe, T. Taniguchi, Z. Papić, J. Hone, and C. R. Dean, [Nature Nanotechnology **15**, 569 \(2020\)](#).
- [34] Y. Kim, D. S. Lee, S. Jung, V. Skákalová, T. Taniguchi, K. Watanabe, J. S. Kim, and J. H. Smet, [Nano Letters **15**, 7445 \(2015\)](#).
- [35] J. K. Jain, [Annual Review of Condensed Matter Physics **6**, 39 \(2015\)](#).
- [36] J. K. Jain, *Composite fermions* (Cambridge University Press, 2007).
- [37] B. I. Halperin, P. A. Lee, and N. Read, [Phys. Rev. B **47**, 7312 \(1993\)](#).

- [38] S. He, S. Das Sarma, and X. C. Xie, *Phys. Rev. B* **47**, 4394 (1993).
- [39] J. Shabani, T. Gokmen, and M. Shayegan, *Phys. Rev. Lett.* **103**, 046805 (2009).
- [40] J. Shabani, T. Gokmen, Y. T. Chiu, and M. Shayegan, *Phys. Rev. Lett.* **103**, 256802 (2009).
- [41] T. Zhao, W. N. Faugno, S. Pu, A. C. Balram, and J. K. Jain, *Phys. Rev. B* **103**, 155306 (2021).
- [42] S. K. Singh, C. Wang, C. T. Tai, C. S. Calhoun, K. A. Villegas Rosales, P. T. Madathil, A. Gupta, K. W. Baldwin, L. N. Pfeiffer, and M. Shayegan, *Nature Physics* **20**, 1247 (2024).
- [43] A. Sharma, A. C. Balram, and J. K. Jain, *Phys. Rev. B* **109**, 035306 (2024).
- [44] M. R. Peterson and C. Nayak, *Phys. Rev. B* **87**, 245129 (2013).
- [45] C. Wang, A. Gupta, S. K. Singh, Y. J. Chung, L. N. Pfeiffer, K. W. West, K. W. Baldwin, R. Winkler, and M. Shayegan, *Phys. Rev. Lett.* **129**, 156801 (2022).
- [46] T. Zhao, A. C. Balram, and J. K. Jain, *Phys. Rev. Lett.* **130**, 186302 (2023).
- [47] R. Kumar, A. Haug, J. Kim, M. Yutushui, K. Khudiyakov, V. Bhardwaj, A. Ilin, K. Watanabe, T. Taniguchi, D. F. Mross, and Y. Ronen, *Quarter- and half-filled quantum hall states and their competing interactions in bilayer graphene* (2024), [arXiv:2405.19405 \[cond-mat.mes-hall\]](https://arxiv.org/abs/2405.19405).
- [48] A. Kumar, W. Escoffier, J. M. Pomirol, C. Faugeras, D. P. Arovas, M. M. Fogler, F. Guinea, S. Roche, M. Goiran, and B. Raquet, *Phys. Rev. Lett.* **107**, 126806 (2011).
- [49] L. C. Campos, T. Taychatanapat, M. Serbyn, K. Surakitbovorn, K. Watanabe, T. Taniguchi, D. A. Abanin, and P. Jarillo-Herrero, *Phys. Rev. Lett.* **117**, 066601 (2016).
- [50] M. Koshino and E. McCann, *Phys. Rev. B* **83**, 165443 (2011).
- [51] K. Zollner, M. Gmitra, and J. Fabian, *Phys. Rev. B* **105**, 115126 (2022).
- [52] M. Levin and B. I. Halperin, *Phys. Rev. B* **79**, 205301 (2009).
- [53] M. Levin, B. I. Halperin, and B. Rosenow, *Phys. Rev. Lett.* **99**, 236806 (2007).
- [54] P. T. Zucker and D. E. Feldman, *Phys. Rev. Lett.* **117**, 096802 (2016).
- [55] L. Wang, I. Meric, P. Y. Huang, Q. Gao, Y. Gao, H. Tran, T. Taniguchi, K. Watanabe, L. M. Campos, D. A. Muller, J. Guo, P. Kim, J. Hone, K. L. Shepard, and C. R. Dean, *Science* **342**, 614 (2013), <https://www.science.org/doi/pdf/10.1126/science.1244358>.
- [56] S. Kaur, T. Chanda, K. R. Amin, D. Sahani, K. Watanabe, T. Taniguchi, U. Ghorai, Y. Gefen, G. J. Sreejith, and A. Bid, *Nature Communications* **15**, 8535 (2024).
- [57] F. Pizzocchero, L. Gammelgaard, B. S. Jessen, J. M. Caridad, L. Wang, J. Hone, P. Bøggild, and T. J. Booth, *Nature Communications* **7**, 11894 (2016).

- [58] M. K. Jat, P. Tiwari, R. Bajaj, I. Shitut, S. Mandal, K. Watanabe, T. Taniguchi, H. R. Krishnamurthy, M. Jain, and A. Bid, *Nature Communications*, 2335 (2024).
- [59] M. Yutushui, M. Hermanns, and D. F. Mross, *Phys. Rev. B* **110**, 165402 (2024).
- [60] R. de Gail, N. Regnault, and M. O. Goerbig, *Phys. Rev. B* **77**, 165310 (2008).
- [61] S. H. Simon and A. C. Balram, *Phys. Rev. B* **111**, 045102 (2025).
- [62] M. Serbyn and D. A. Abanin, *Phys. Rev. B* **87**, 115422 (2013).
- [63] A. A. Zibrov, P. Rao, C. Kometter, E. M. Spanton, J. I. A. Li, C. R. Dean, T. Taniguchi, K. Watanabe, M. Serbyn, and A. F. Young, *Phys. Rev. Lett.* **121**, 167601 (2018).
- [64] Y. Chen, Y. Huang, Q. Li, B. Tong, G. Kuang, C. Xi, K. Watanabe, T. Taniguchi, G. Liu, Z. Zhu, L. Lu, F.-C. Zhang, Y.-H. Wu, and L. Wang, *Nature Communications* **15**, 6236 (2024).
- [65] M. Kharitonov, *Phys. Rev. B* **85**, 155439 (2012).
- [66] J. Alicea and M. P. A. Fisher, *Phys. Rev. B* **74**, 075422 (2006).
- [67] A. A. Zibrov, E. M. Spanton, H. Zhou, C. Kometter, T. Taniguchi, K. Watanabe, and A. F. Young, *Nature Physics* **14**, 930 (2018).
- [68] B. E. Feldman, A. J. Levin, B. Krauss, D. A. Abanin, B. I. Halperin, J. H. Smet, and A. Yacoby, *Phys. Rev. Lett.* **111**, 076802 (2013).
- [69] C. Cong, T. Yu, K. Sato, J. Shang, R. Saito, G. F. Dresselhaus, and M. S. Dresselhaus, *ACS Nano* **5**, 8760 (2011).
- [70] T. A. Nguyen, J.-U. Lee, D. Yoon, and H. Cheong, *Scientific Reports* **4**, 4630 (2014).
- [71] P. Tiwari, S. K. Srivastav, and A. Bid, *Phys. Rev. Lett.* **126**, 096801 (2021).
- [72] S. K. Srivastav, A. Udupa, K. Watanabe, T. Taniguchi, D. Sen, and A. Das, *Phys. Rev. Lett.* **132**, 096301 (2024).
- [73] D. A. Abanin, B. E. Feldman, A. Yacoby, and B. I. Halperin, *Phys. Rev. B* **88**, 115407 (2013).